Article

Effects of Sintering Conditions on Giant Dielectric and Nonlinear Current–Voltage Properties of TiO$_2$-Excessive Na$_{1/2}$Y$_{1/2}$Cu$_3$Ti$_{4.1}$O$_{12}$ Ceramics

Pariwat Saengvong [1], Jakkree Boonlakhorn [2], Narong Chanlek [3], Nutthakritta Phromviyo [1], Viyada Harnchana [1], Pairot Moontragoon [1], Pornjuk Srepusharawoot [1], Sriprajak Krongsuk [1] and Prasit Thongbai [1,*]

[1] Giant Dielectric and Computational Design Research Group (GD–CDR), Department of Physics, Faculty of Science, Khon Kaen University, Khon Kaen 40002, Thailand
[2] Department of Basic Science and Mathematics, Faculty of Science, Thaksin University, Songkhla 90000, Thailand
[3] Synchrotron Light Research Institute (Public Organization), 111 University Avenue, Muang District, Nakhon Ratchasima 30000, Thailand
[*] Correspondence: pthongbai@kku.ac.th

Abstract: The effects of the sintering conditions on the phase compositions, microstructure, electrical properties, and dielectric responses of TiO$_2$-excessive Na$_{1/2}$Y$_{1/2}$Cu$_3$Ti$_{4.1}$O$_{12}$ ceramics prepared by a solid-state reaction method were investigated. A pure phase of the Na$_{1/2}$Y$_{1/2}$Cu$_3$Ti$_{4.1}$O$_{12}$ ceramic was achieved in all sintered ceramics. The mean grain size slightly increased with increasing sintering time (from 1 to 15 h after sintering at 1070 °C) and sintering temperature from 1070 to 1090 °C for 5 h. The primary elements were dispersed in the microstructure. Low dielectric loss tangents (tan δ~0.018–0.022) were obtained. Moreover, the dielectric constant increased from ε'~5396 to 25,565 upon changing the sintering conditions. The lowest tan δ of 0.009 at 1 kHz was obtained. The electrical responses of the semiconducting grain and insulating grain boundary were studied using impedance and admittance spectroscopies. The breakdown voltage and nonlinear coefficient decreased significantly as the sintering temperature and time increased. The presence of Cu$^+$, Cu^{3+}, and Ti^{3+} was examined using X-ray photoelectron spectroscopy, confirming the formation of semiconducting grains. The dielectric and electrical properties were described using Maxwell–Wagner relaxation, based on the internal barrier layer capacitor model.

Keywords: giant/colossal dielectric permittivity; varistor; admittance spectroscopy; impedance spectroscopy; Maxwell–Wagner polarization

1. Introduction

Dielectric materials are among the most interesting materials for use in electronic devices such as capacitors and high-energy storage devices [1,2]. CaCu$_3$Ti$_4$O$_{12}$ (CCTO) has been extensively studied because CCTO can exhibit a high dielectric constant ($\varepsilon' > 10^4$) [3–8]. Furthermore, CCTO ceramic is not a ferroelectric material. The observed large ε' value was stable with respect to temperature and frequency. However, the dielectric loss tangent remains too high (tan δ > 0.1) and cannot be applied to electronic devices. Many years ago, researchers attempted to improve the dielectric properties of CCTO by increasing ε', reducing tan δ, and increasing the efficiency of dielectric properties for stability with temperature and frequency [6,7,9,10]. It is believed that the origin of the dielectric properties of CCTO arises from its microstructure, consisting of an insulating grain boundary (i-GBs) and a semiconducting grain (semi-G). This microstructure is called an internal barrier layer capacitor (IBLC) structure [3,11].

In the IBLC model, tan δ can be reduced by increasing the grain boundary resistance (R$_{gb}$) [12,13]. In 2006, Y. Lin et al. reduced the tan δ in CCTO from 0.07 to 0.03 by adding

composite TiO_2 into samples [9]. When the R_{gb} was analyzed using impedance spectroscopy, it appeared that R_{gb} increased with increasing TiO_2 contents in CCTO ceramics. Moreover, the breakdown electric field (E_b) of the nonlinear J-E characteristics increased with increasing TiO_2 contents, indicating that R_{gb} can be increased by adding TiO_2 to CCTO ceramics, resulting in a decrease in tan δ, which corresponds to the IBCL model [9,14].

The optimized sintering condition is one technique that has been used to improve dielectric properties, which can modify the microstructure of ceramics. The effect of sintering temperature results in grain size changes and i-GBs. Generally, ε' can be increased by increasing the temperature and duration of sintering in $ACu_3Ti_4O_{12}$ ceramics [11,15–17].

$ACu_3Ti_4O_{12}$ is a dielectric material group that has received extensive attention because of its interesting dielectric properties. $CaCu_3Ti_4O_{12}$ (CCTO) [4,5], $CdCu_3Ti_4O_{12}$ (CdCTO) [18,19], $Na_{1/2}Sm_{1/2}Cu_3Ti_4O_{12}$ (NSmCTO) [20], $Na_{1/2}Y_{1/2}Cu_3Ti_4O_{12}$ (NYCTO) [16,21–23], $Na_{1/2}La_{1/2}Cu_3Ti_4O_{12}$ (NLCTO) [24,25], $Y_{2/3}Cu_3Ti_4O_{12}$ (YCTO) [26,27], $La_{2/3}Cu_3Ti_4O_{12}$ (LCTO) [28], $Bi_{2/3}Cu_3Ti_4O_{12}$ (BCTO) [29–32], and $Na_{1/2}Bi_{1/2}Cu_3Ti_4O_{12}$ (NBCTO) [17,33,34] were dielectric materials in the $ACu_3Ti_4O_{12}$ oxides group. These materials have perovskite structures and often have reported excellent dielectric properties. However, these materials still have limitations under many conditions for application in electronic devices. The dielectric properties of CCTO and NYCTO ceramics can be significantly improved by the addition of excess TiO_2 [9,21].

Most recently, the tan δ value of $Na_{1/2}Y_{1/2}Cu_3Ti_{4.1}O_{12}$ can be significantly reduced (tan δ < 0.1), while the ε' value is still larger than 10^4. The improved dielectric properties were attributed to the enhanced electrical properties of the i-GBs due to the excessive TiO_2-rich phase boundaries, which are also associated with the oxygen content along the i-GBs. Generally, the giant dielectric properties of CCTO-based materials are closely related to sintering conditions [5,35,36]. Thus, the giant dielectric properties can be optimized by tuning the sintering conditions. It is hypothesized that the dielectric properties of $Na_{1/2}Y_{1/2}Cu_3Ti_{4.1}O_{12}$ can be further improved by varying the sintering conditions. The optimization of fabrication conditions is one of the most important topics for developing materials used in electronic devices. This is the motivation of this work. Hence, the aim of this study was to investigate the effect of sintering conditions on the dielectric properties of $Na_{1/2}Y_{1/2}Cu_3Ti_{4.1}O_{12}$ to optimize the dielectric properties.

In this study, the effects of sintering conditions on the dielectric and electrical properties of $Na_{1/2}Y_{1/2}Cu_3Ti_{4.1}O_{12}$ ceramics were investigated. The phase composition and microstructure were analyzed. Significant improvements in the dielectric and electrical behaviors with respect to ε' and tan δ were achieved. The origin of the observed dielectric and electrical properties is described.

2. Experimental Details

$Na_{1/2}Y_{1/2}Cu_3Ti_{4.1}O_{12}$ powder was prepared using the solid-state reaction method (SSR). The starting materials were Na_2CO_3 (Sigma-Aldrich, St. Louis, MO, USA, 99.9%), Y_2O_3 (CERAC, 99.99%), CuO (Sigma-Aldrich, St. Louis, MO, USA, 99.9%), and TiO_2 (Sigma-Aldrich, St. Louis, MO, USA, 99.9%). The powders were mixed using a ball milling method for 24 h. The powder was calcined at 1000 °C in air for 10 h at heating and cooling rates of 5 °C/min. The calcined powder was finely crushed and compressed into pellets for sintering. The first set of pellets was sintered at 1070 °C for 1, 5, and 15 h. The second set of pellets was sintered at 1080 and 1090 °C for 5 h. The samples produced under these conditions are referred to as 1NYCTTiO, 2NYCTTiO, 3NYCTTiO, 4NYCTTiO, and 5NYCTTiO, respectively.

The phase compositions were analyzed by X-ray diffraction (XRD, PANalytical, EMPYREAN). The XRD patterns were measured in the 2θ range of 25–70°, and the lattice parameters were calculated using the Rietveld technique. The surfaces of the ceramics were characterized by scanning electron microscopy (SEM, SEC, SNE-4500 M). The element distributions were analyzed using a mapping technique, and field emission scanning electron microscopy (FIB-FESEM) was used for SEM mapping. X-ray photoemission spectroscopy

(XPS, PHI5000 Versarobe II, ULVAC-PHI) was used to analyze the oxidation states of the $Na_{1/2}Y_{1/2}Cu_3Ti_{4.1}O_{12}$ ceramics. The densities of the sintered samples were measured.

To determine the dielectric and electrical properties, the as-sintered ceramics were polished to a smooth surface. Next, parallel-plate electrodes were made by painting Ag paste on both sides of the smooth surfaces. Then, the sample with top and bottom electrodes was heated in air at 600 °C for 30 min. The area of the top and bottom electrodes was 2.83 cm^2. The capacitance (C_p) and tanδ were measured in the frequency range of 10^2 to 10^6 Hz at room temperature using an impedance analyzer (KEYSIGHT E4990A). The amplitude of the ac field was 0.5 V. In addition, the dielectric behavior was studied in the temperature range of −60 to 210 °C. Finally, the nonlinear electrical (I–V) properties were diagnosed using a high-voltage measurement unit (Keithley 247 model).

The ε' value was calculated by the equation:

$$\varepsilon' = \frac{C_p t}{\varepsilon_0 S} \tag{1}$$

where ε_0 is the permittivity of free space and S and t are the electrode area and sample thickness, respectively. The complex dielectric permittivity (ε^*) was used to calculate the complex impedance (Z*) using Equation (2).

$$\varepsilon^* = \varepsilon' - i\,\varepsilon'' = (i\omega C_0 Z^*)^{-1} = \left[i\omega C_0 \left(Z' - i\,Z'' \right) \right]^{-1} \tag{2}$$

where Z′ and Z″ are the real part and imaginary part of Z*, respectively, ε' and ε'' are the real and imaginary parts of ε^*, $C_0 = \varepsilon_0 A/d$ is the empty cell capacitance, $\tan\delta = \varepsilon''/\varepsilon'$, and ω is the angular frequency ($\omega = 2\pi f$).

3. Results and Discussion

The XRD characteristics of the sintered $Na_{1/2}Y_{1/2}Cu_3Ti_{4.1}O_{12}$ ceramics were analyzed. Accordingly, the lattice parameters were calculated using the Rietveld technique. Figure 1 shows the XRD patterns of all samples, showing the pure phase (not detecting the second phase and not detecting the TiO$_2$ phase) with the perovskite structure (JCPDS 75–2188). The lattice parameters of 1NYCTTiO, 2NYCTTiO, 3NYCTTiO, 4NYCTTiO, and 5NYCTTiO were 7.383(8), 7.383(2), 7.382(8), 7.385(4), and 7.386(4) Å, respectively. The sintering conditions did not affect the lattice parameters of the $Na_{1/2}Y_{1/2}Cu_3Ti_{4.1}O_{12}$ ceramics. Moreover, the XRD patterns and lattice parameters were comparable to the XRD spectra that were reported for $Na_{1/2}Y_{1/2}Cu_3Ti_4O_{12}$ (NYCTO) ceramics [16,21–23].
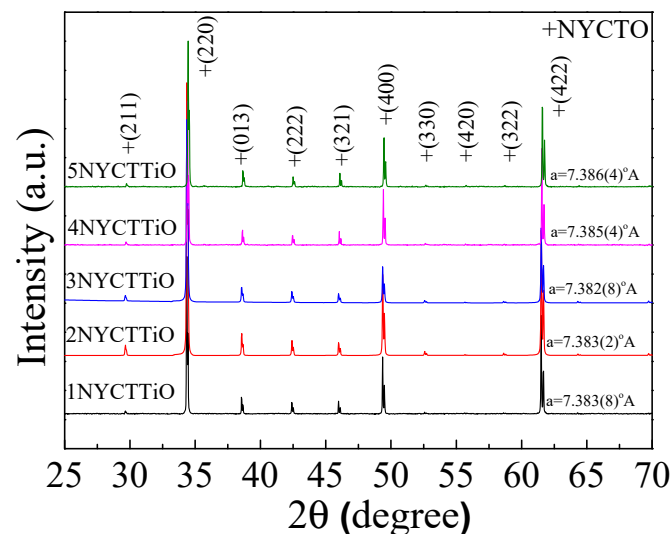

Figure 1. XRD patterns of the $Na_{1/2}Y_{1/2}Cu_3Ti_{4.1}O_{12}$ ceramics sintered at 1070 °C for 1, 5, and 15 h and sintered at 1080 and 1090 °C for 5 h.

Figure 2a–e show the morphologies of $Na_{1/2}Y_{1/2}Cu_3Ti_{4.1}O_{12}$ ceramics sintered under different conditions using the SEM technique. The SEM images clearly show the grains and GBs. A small number of pores can be observed. The grain-size distributions are shown in Figure 2f–j. The mean grain sizes of the 1NYCTTiO, 2NYCTTiO, 3NYCTTiO, 4NYCTTiO, and 5NYCTTiO samples were 3.55 ± 1.46, 3.63 ± 1.59, 4.06 ± 1.55, 3.66 ± 1.61, and 3.90 ± 1.59 μm, respectively. The average grain size increased slightly with increasing temperature and time in the sintering process, which may have been caused by the enhanced diffusion of ions [6,7]. The densities of the samples were 96.34, 97.40, 97.67, 95.61, and 96.90%, respectively.
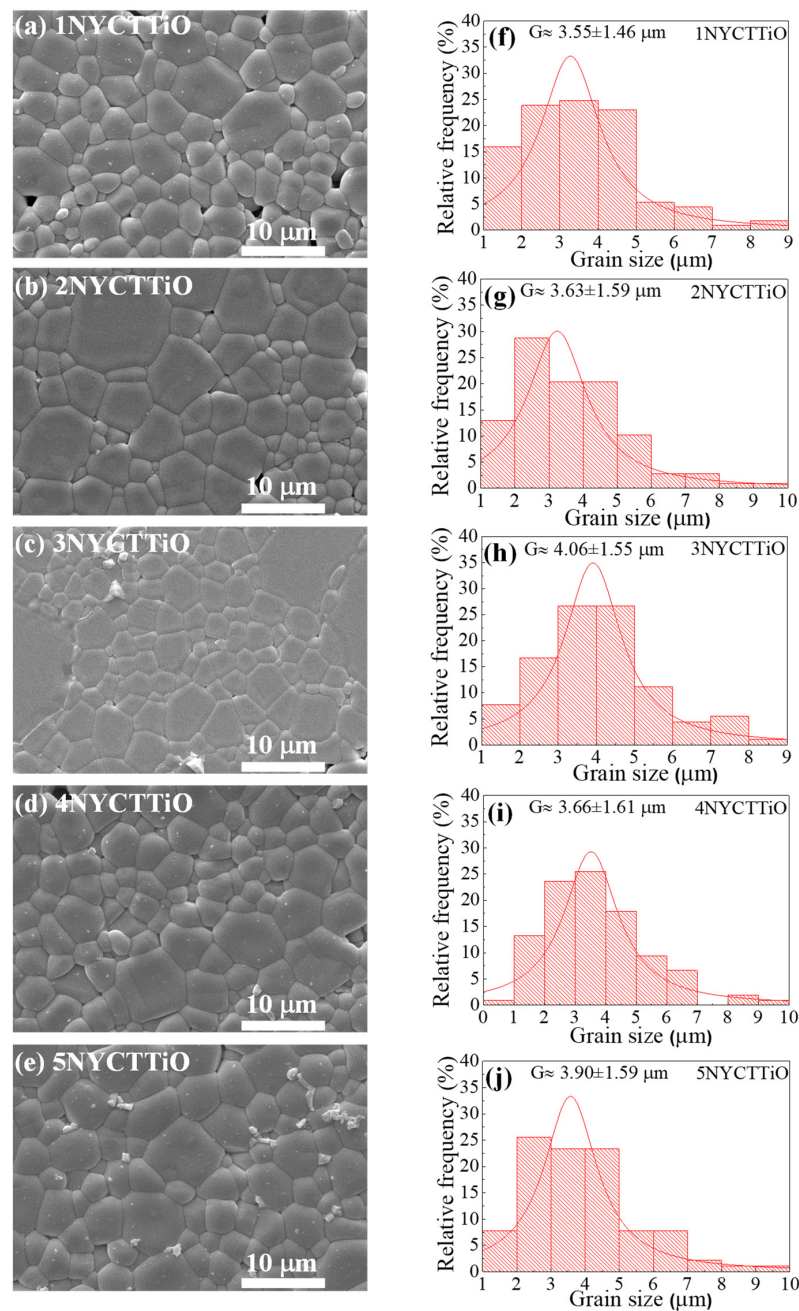

Figure 2. SEM images of polished surfaces of $Na_{1/2}Y_{1/2}Cu_3Ti_{4.1}O_{12}$ ceramics sintered at (**a**) 1070 °C for 1 h, (**b**) 1070 °C for 5 h, (**c**) 1070 °C for 15 h, (**d**) 1080 °C for 5 h, and (**e**) 1090 °C for 5 h and grain size distributions with sintering at (**f**) 1070 °C for 1 h, (**g**) 1070 °C for 5 h, (**h**) 1070 °C for 15 h, (**i**) 1080 °C for 5 h, and (**j**) 1090 °C for 5 h.

The elemental composition of the $Na_{1/2}Y_{1/2}Cu_3Ti_{4.1}O_{12}$ ceramic sintered at 1070 °C for 15 h was studied using EDS. The EDS spectrum shown in Figure 3 can be used to observe the major elements consisting of Na, Y, Cu, Ti, and O peaks to confirm the elemental composition of the ceramics. The mapping technique was used to study the elemental distribution, as shown in Figure 4a,b. All elements were homogeneously dispersed inside the grains. Figure 4a shows the distribution of elements; all elements were well-distributed throughout the sample. However, segregation of Cu was observed around the GB to detect CuO, which may have been caused by the effect of sintering temperature and increasing Ti concentration. The concentration of excess Ti may enter into the Cu sites in the structure, causing the segregation of CuO at the GB during the temperature sintering process [9–11]. Moreover, when examining the distribution of elements at the GB in the area without CuO, Ti element was detected at the GB, indicating that excess Ti tends to unite at the GB, as shown in Figure 4b. Generally, TiO_2 and CuO have electrical insulating properties; detecting this at the GB may result in an increase in resistance at the GB, which is an important factor for reducing tanδ in perovskite dielectric materials [10].
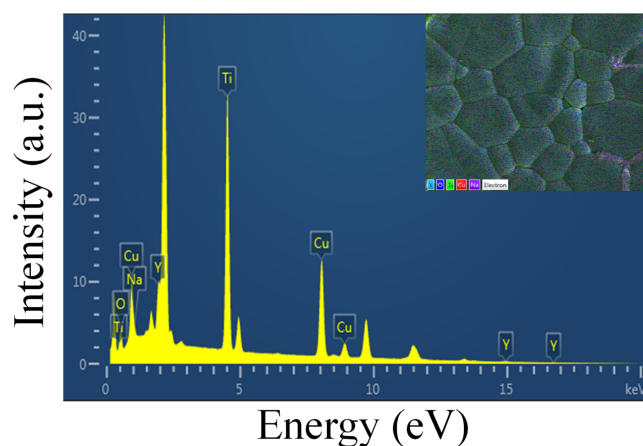

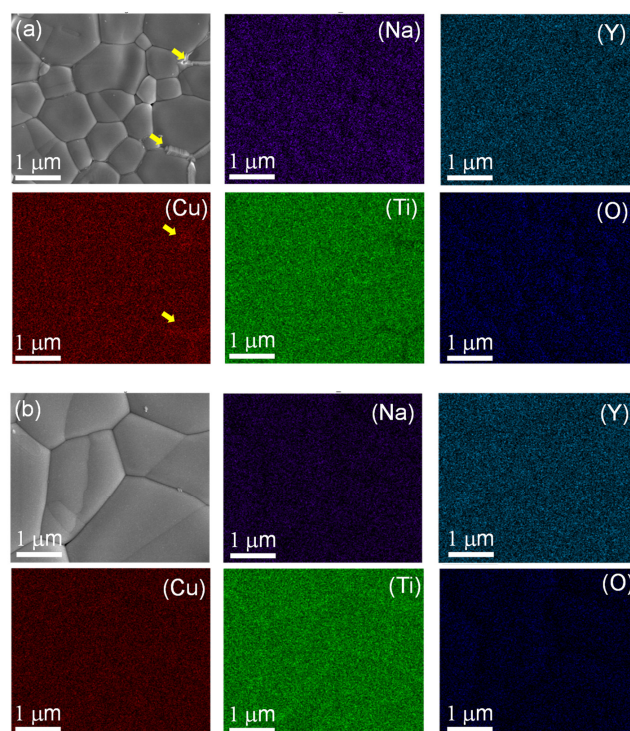**Figure 3.** EDS spectrum of $Na_{1/2}Y_{1/2}Cu_3Ti_{4.1}O_{12}$ ceramic sintered at 1070 °C for 15 h.

Figure 4. SEM mapping images of Na, Y, Cu, Ti, and O considering the amount of Cu (**a**) and Ti (**b**) at the grain boundary of the $Na_{1/2}Y_{1/2}Cu_3Ti_{4.1}O_{12}$ ceramic sintered at 1070 °C for 15 h.

Depending on the frequency shown in Figure 5a, the ε' values at 1 kHz and 20 °C for the 1NYCTTiO, 2NYCTTiO, 3NYCTTiO, 4NYCTTiO, and 5NYCTTiO samples were 5396, 8370, 25,565, 9972, and 8896, respectively. The ε' values tended to increase with increasing sintering duration and slightly increased with increasing sintering temperature, which might be a result of the increasing grain size when this result was considered using the IBLC model [6,15–18]. It was also observed that ε' was a relatively stable frequency. However, at a high frequency (>10^5 Hz), ε' rapidly dropped because of the dielectric relaxation process. Moreover, all the samples had a low tan δ (<0.05) over the frequency range of 70–100 kHz. tan δ slightly changed with increasing sintering duration and sintering temperature. The tan δ values of the samples were 0.009, 0.018, 0.022, 0.024, and 0.025, respectively, as observed in Figure 5b. However, tan δ increased rapidly at frequencies higher than 10^5 Hz. This is the dielectric relaxation response, which is related to the fast ε' drop at high frequencies. These behaviors are similar to the dielectric behaviors that occur in CCTO and NYCTO ceramics [1–8]. The dielectric relaxation at high frequencies was caused by the fact that the electric dipole cannot complete the polarization process because the relaxation time is too small.
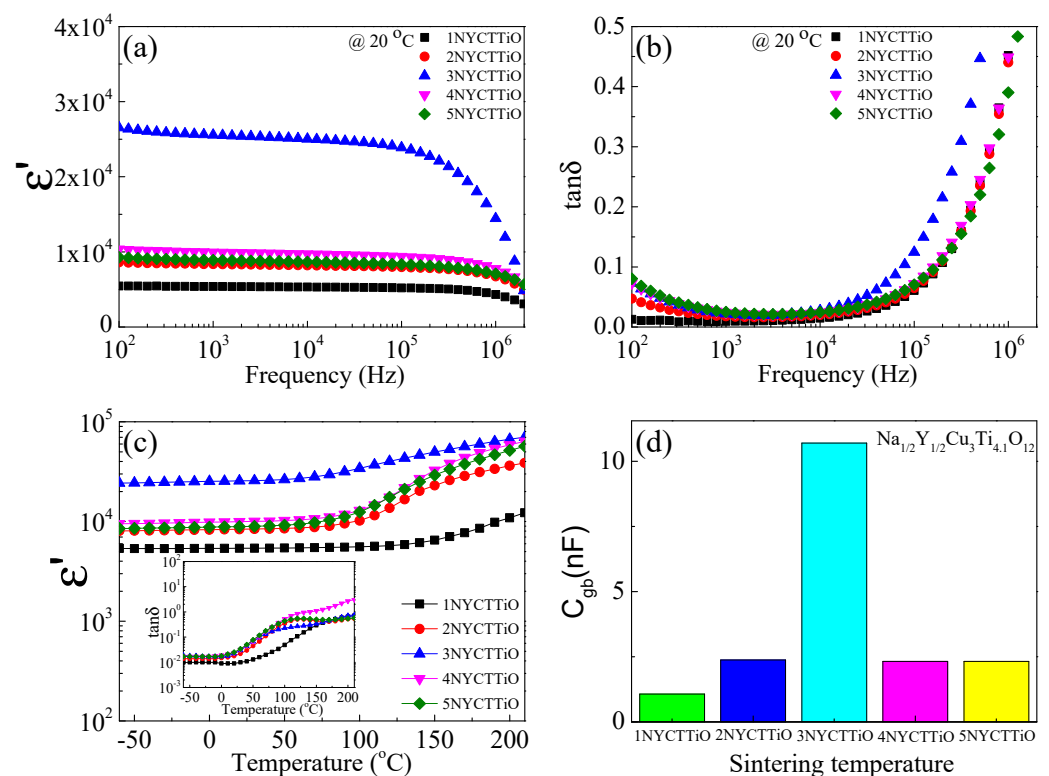

Figure 5. (**a**) Dielectric constant (ε') and (**b**) dielectric loss tangent (tanδ) at room temperature (20 °C) as a function of frequency for $Na_{1/2}Y_{1/2}Cu_3Ti_{4.1}O_{12}$ ceramics sintered under different conditions. (**c**) Dielectric constant (ε') and (inset) dielectric loss tangent (tanδ) as a function of temperature in the range of −60 to 210 °C. (**d**) Grain-boundary capacitance (C_{gb}).

Figure 5c shows the dependence of ε' and tan δ on the temperature. The ε' and tan δ values of the 2NYCTTiO, 4NYCTTiO, and 5NYCTTiO samples were greatly increased when the temperature was above 90 °C. These dielectric responses were caused by the electric charge having high energy (maybe more than the potential energy at the GB) and being easier to move at a high temperature. As a result, the polarization process occurs more easily and the electrical conductivity increases [19–22]. However, the ε' values of the 1NYCTTiO and 3NYCTTiO samples were relatively stable with temperature, indicating that the sintering condition for ε' stability with temperature was successfully achieved. As shown in Figure 5d, the GB capacitance (C_{gb}) values were calculated in the temperature range of 150–200 °C using the electric modulus (M*) technique. The C_{gb} values of the

1NYCTTiO, 2NYCTTiO, 3NYCTTiO, 4NYCTTiO, 5NYCTTiO samples were 1.07, 2.38, 10.7, 2.32, and 2.32 nF, respectively. The C_{gb} values did not change with increasing sintering temperatures due to the small change in the sintering temperature. However, C_{gb} tended to increase with increasing sintering duration, which corresponds to an increase in ε'. This may be the major factor causing the ε' rise when using the IBLC model [6]. In this study, excellent dielectric properties were obtained for the 3NYCTTiO samples.

The excellent dielectric properties of NYCTO are attributed to the electrically the heterogeneous microstructure of the materials. These microstructures consist of i-GBs (high resistance) and semi-Gs (low resistance). The electrical circuit model explained the electrical conductivity of the materials, which consisted of a capacitor (C) and a resistor (R) connected in series (RC circuits). Thus, impedance spectroscopy was used to analyze the electrical properties of the ceramic materials. Normally, the grain resistance (R_g) and GB resistance (R_{gb}) are obtained by the small semicircle (or nonzero intercept) and large semicircle observed from Z* plots, respectively. Moreover, the grain capacitance (C_g) and GB capacitance (C_{gb}) can be calculated using impedance spectroscopy [2,23]. Z^* is calculated using Equation (3).

$$Z^* = Z' - iZ'' = \frac{1}{R_g^{-1} + i\omega C_g} + \frac{1}{R_{gb}^{-1} + i\omega C_{gb}} \tag{3}$$

Figure 6a shows the impedance complex plane (Z*) plots of the 1NYCTTiO, 2NYCTTiO, 3NYCTTiO, 4NYCTTiO, and 5NYCTTiO samples. The large semicircle tended to decrease with increasing sintering duration and slightly decreased with increasing sintering temperature, indicating that R_{gb} tended to decrease with increasing sintering duration and sintering temperature. Moreover, the R_g tended to decrease with increasing sintering duration (R_g was trivially changed with increasing sintering temperature) when observed from the non-zero intercept in the inset of Figure 6a. The effects of changing the R_g and R_{gb} on the dielectric properties were investigated.
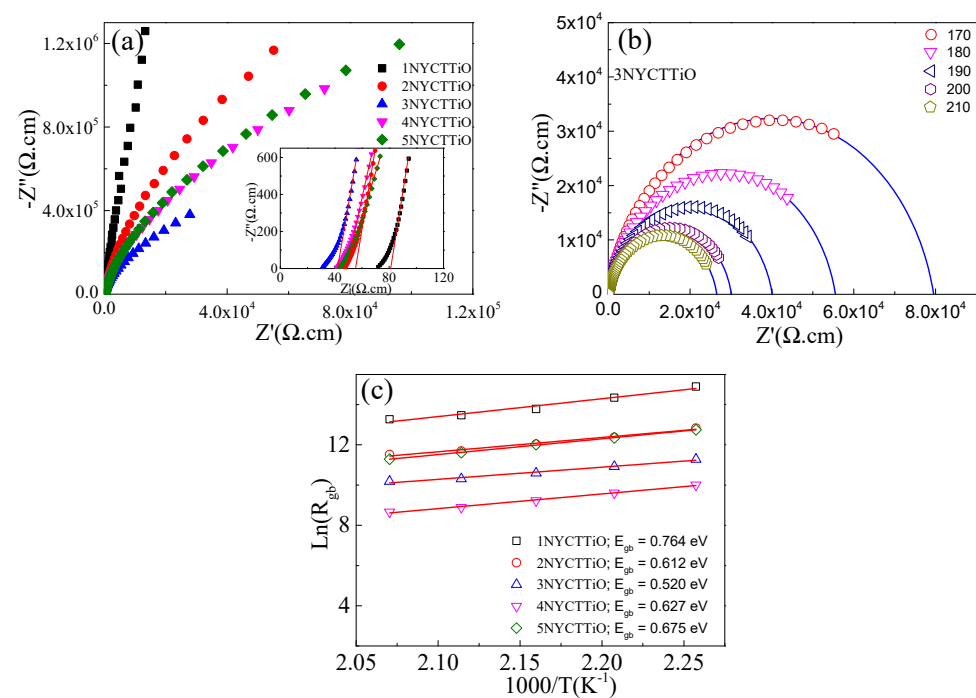

Figure 6. (**a**) Impedance complex plane plot at 20 °C and inset non-zero intercept of $Na_{1/2}Y_{1/2}Cu_3Ti_{4.1}O_{12}$ ceramics sintered at 1070 °C for 1, 5, and 15 h and sintered at 1080 and 1090 °C for 5h. (**b**) Impedance complex plane plot in the temperature range of 170–210 °C for the sample sintered at 1070 °C for 15 h. (**c**) Arrhenius plot of the grain boundary conductivity (R_{gb}).

To calculate the activation at the GB (E_{gb}), R_{gb} was obtained by fitting the Z* data with the IBLC model at various temperatures. For the IBLC structure of CCTO-based ceramics, the microstructure consisted of i-GBs and semi-G [3]. Generally, the C_{gb} values of the ceramics were much higher than their C_g values ($C_{gb} \gg C_g$). Therefore, Equation (3) can be modified to create a fitting model as follows [9]:

$$Z^* = R_g + \frac{R_{gb}}{1 + \left(i\omega R_{gb}C_{gb}\right)^{\alpha}} \tag{4}$$

where α is a constant ($0 < \alpha \leq 1$). The R_{gb} values were obtained by fitting the experimental data of Z* in the temperature range of 170–210 °C. Figure 6b shows the fitted results of Z* plots for the 3NYCTTiO sample for calculating the E_{gb} value. The other samples were fitted using the same process (data not shown). Next, the E_{gb} values were calculated using the Arrhenius law:

$$R_{gb} = R_0 \exp\left(\frac{E_{gb}}{k_B T}\right) \tag{5}$$

where k_B is the Boltzmann constant, T is the temperature (Kelvins), and R_0 is a pre-exponential constant term. As shown in Figure 6c, the E_{gb} values of 1NYCTTiO, 2NYCTTiO, 3NYCTTiO, 4NYCTTiO, and 5NYCTTiO were 0.764, 0.612, 0.520, 0.627, and 0.675 eV, respectively. The E_{gb} values tended to decrease with increasing sintering durations, but the E_{gb} values trivially changed with increasing sintering temperatures, similar to R_{gb}. The E_{gb} values of all samples were close to those reported for CCTO and NYCTO ceramics (≈ 0.6 eV), confirming that the GBs of the samples were electrically insulating [1,6,24,25]. Furthermore, the decrease in the E_{gb} values might be caused by an increase in the number of oxygen vacancies.

To study the dielectric properties of $Na_{1/2}Y_{1/2}Cu_3Ti_{4.1}O_{12}$ and other $ACu_3Ti_4O_{12}$ compounds, the conductivity of the semi-Gs was considered to be an important factor. Generally, R_g is calculated from the nonzero intercept on the Z'-axis in the Z* plot. The conductivity of the semi-Gs was confirmed by calculating the E_g value (activation energy in the grain). In this study, E_g was calculated using admittance spectroscopy (Y*). According to the IBLC model, for the equivalent circuit (RC), when $R_g \ll R_{gb}$ and $C_g \ll C_{gb}$, the electrical conductivity can be analyzed using Equation (6):

$$Y^* = \frac{\left(1 - \omega^2 \tau_g \tau_{gb} + i\omega\tau_{gb}\right)\left(R_{gb}^{-1}\right)}{1 + i\omega\tau} \tag{6}$$

where $Y^* = \left(1 + i\omega R_g C_g\right)/R_g$ and $Y^* = \left(1 + i\omega R_{gb}C_{gb}\right)/R_{gb}$. $\tau = R_g C_{gb}$, $\tau_g = R_g C_g$, and $\tau_{gb} = R_{gb}C_{gb}$. When using Equation (6), this equation can be reduced to $R_g = 1/2Y''_{max}$, where Y''_{max} is the maximum value at Y''-peak. The Y''_{max} values of the 1NYCTTiO, 2NYCTTiO, 3NYCTTiO, 4NYCTTiO, and 5NYCTTiO samples are shown in Figure 7a–e. In addition, the E_g values were calculated using the Arrhenius law:

$$\sigma_g = \sigma_0 e^{\left(\frac{-E_g}{k_B T}\right)} \tag{7}$$

where E_g is the activation energy for the conductivity in the grain. The E_g values were calculated in the temperature range from −60 to 0 °C, as shown in Figure 7f. The E_g values of 1NYCTTiO, 2NYCTTiO, 3NYCTTiO, 4NYCTTiO, and 5NYCTTiO were 0.126, 0.119, 0.114, 0.117, and 0.116 eV, respectively. The E_g values were close to those reported for NYCTO ceramics, indicating that the grain was a semiconductor [5,6,8,26,27]. Moreover, E_g tends to decrease slightly with increasing sintering duration (E_g is trivially changed with increasing sintering temperatures), and the sintering duration corresponds to a decrease in R_g. The reductions in E_g and R_g correspond to an increase in ε', which is an important factor for explaining the dielectric properties of $Na_{1/2}Y_{1/2}Cu_3Ti_{4.1}O_{12}$ ceramics. The relationship

between the dielectric permittivity and the electrical conductivity of the semi-Gs and i-GBs is presented in Table 1.
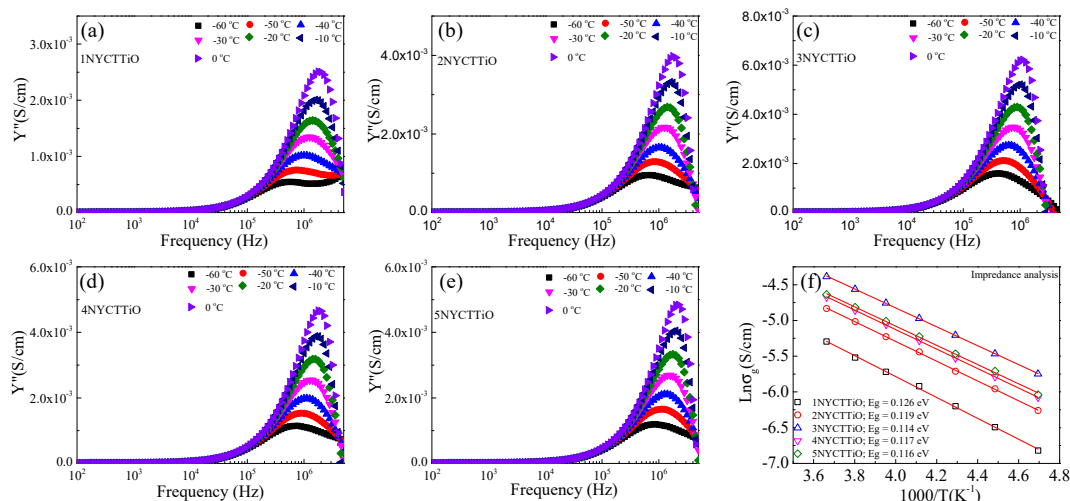

Figure 7. Admittance imaginary (Y″) as a function of the frequency plot in the temperature range of −60–0 °C for $Na_{1/2}Y_{1/2}Cu_3Ti_{4.1}O_{12}$ ceramics sintered at (**a**) 1070 °C for 1 h, (**b**) 1070 °C for 5 h, (**c**) 1070 °C for 15 h, (**d**) 1080 °C for 5 h, and (**e**) 1090 °C for 5 h. (**f**) Arrhenius plot of grain conductivity (σ_g).

Table 1. ε' at 1 kHz and 20 °C, R_g at 20 °C, and calculated E_g, E_{gb}, and C_{gb} of $Na_{1/2}Y_{1/2}Cu_3Ti_{4.1}O_{12}$ sintered at 1070 °C for 1, 5, and 15 h and sintered at 1080 and 1090 °C for 5 h.

Sample	R_g (Ω)	E_g (eV)	E_{gb} (eV)	C_{gb} (nF)	ε'
1NYCTTiO	83	0.126	0.764	1.07	5396
2NYCTTiO	54	0.119	0.612	2.38	8370
3NYCTTiO	41	0.114	0.520	10.7	25,565
4NYCTTiO	48	0.117	0.627	2.32	9972
5NYCTTiO	49	0.116	0.675	2.32	8896

Normally, the grains of $ACu_3Ti_4O_{12}$ ceramics are semiconducting. Thus, studying the electrical properties of grains plays an important role in changing the dielectric properties of ceramic materials. The oxidation states of the Ti and Cu ions in the grains were investigated using XPS. Figure 8a–d show the electron hopping between $Cu^+ \leftrightarrow Cu^{2+}$, $Cu^{2+} \leftrightarrow Cu^{3+}$, and $Ti^{3+} \leftrightarrow Ti^{4+}$ in the 2NYCTTiO and 3NYCTTiO samples. The peaks of $Cu2p_{3/2}$ were fitted using Gaussian–Lorentzian models, as shown in Figure 8a,b, and the peaks of Cu^+, Cu^{2+}, and Cu^{3+} were observed at the mean binding energies of approximately ≈932.13–932.25, 933.92–934.09, and 935.63–936.10 eV, respectively. The calculated Cu^+/Cu^{2+} of the 2NYCTTiO and 3NYCTTiO samples were 18.34% and 45.62%. The Cu^+/Cu^{2+} ratio tends to increase with increasing sintering durations. Two peaks of Ti $2p_{3/2}$ are shown in Figure 8c,d. The Ti^{3+}/Ti^{4+} ratios were 3.33% and 3.18%, which almost did not change with increasing sintering durations, indicating that the effect of sintering was not affected by electron hopping between $Ti^{3+} \leftrightarrow Ti^{4+}$. Thus, the electrical properties of the grains may result from electron hopping between $Cu^+ \leftrightarrow Cu^{2+}$. Generally, the electrical conductivity depends on the concentration of free charges and the mobility of the charge carriers in the material. $ACu_3Ti_4O_{12}$ ceramics often lose oxygen during sintering, resulting in oxygen vacancies and free electrons [28,29]. Accordingly, increasing the Cu^+/Cu^{2+} ratio indicates an increase in the electrical conductivity of the grains. The increasing electrical conductivity within the grains was related to a decrease in R_g, which may be the major cause of the ε' increase, which can be described based on the IBLC model [30].
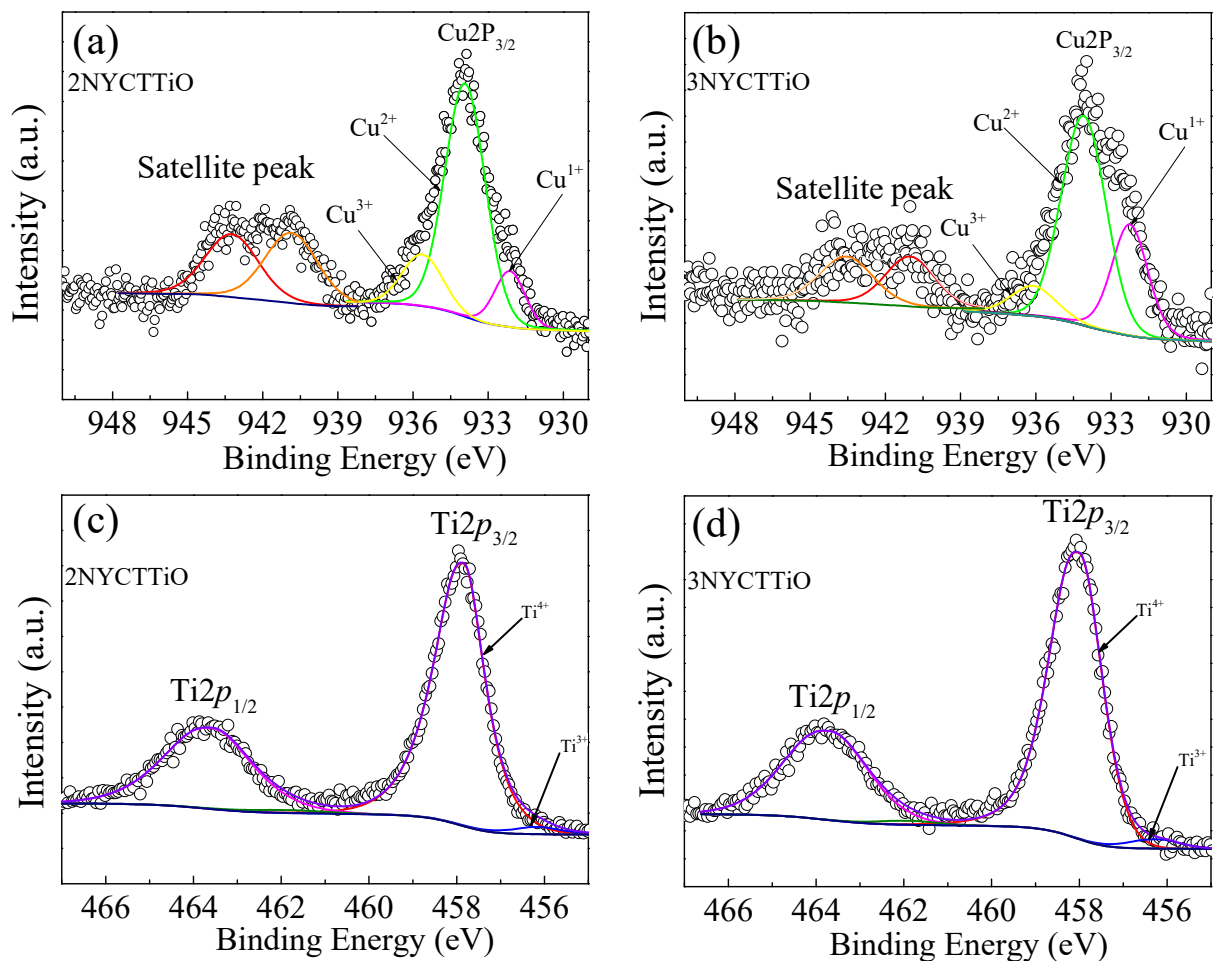
Figure 8. (**a**,**b**) XPS spectra of Cu2p and (**c**,**d**) XPS spectra of $Ti2p_{3/2}$ for $Na_{1/2}Y_{1/2}Cu_3Ti_{4.1}O_{12}$ ceramics sintered at 1070 °C for 5 and 15 h.

The non-ohmic characteristics of $ACu_3Ti_4O_{12}$ ceramics have been extensively studied to explain their electrical behavior in the R_{gb} of materials. The effect of sintering duration on the nonlinear current density–electric field (J–E) characteristics of the $Na_{1/2}Y_{1/2}Cu_3Ti_{4.1}O_{12}$ ceramics is shown in Figure 9. The E_b and the nonlinear coefficient (α) can be calculated. Both values can be calculated using the equation of varistor characteristics ($I = KV^{\alpha}$), where K is the constant related to the resistance of the material. The α values were calculated in the current density (J) range of 1–10 mA, and the E_b values were obtained at $J = 1$ mA. The α and E_b values of the 1NYCTTiO, 2NYCTTiO, 3NYCTTiO, 4NYCTTiO, and 5NYCTTiO samples were 6.1, 5.7, 4.1, 4.2, and 4.7 and 4251.5, 1426.50, 138.2, 1101.2, and 1825.4 V/cm, respectively. The E_b and α values tended to decrease with increasing temperature durations, which is similar to the electrical behavior of NYCTO ceramics [2,6]. Both values support R_{gb} and E_{gb}, which decreased with increasing temperatures. With respect to the sintering temperature effect, E_b was slightly decreased in the 4NYCTTiO sample (sintered at 1080 °C for 5 h) but increased in the 5NYCTTiO sample (sintered at 1090 °C for 5 h) when compared with the 2NYCTTiO sample (sintered at 1070 °C for 5 h). In the 4NYCTTiO sample, the slight decrease in the E_b values may have been caused by the enhancement in the oxygen vacancy concentration at the i-GBs in the sintering temperature mechanism. However, the increased E_b values in the 5NYCTTiO sample may have been caused by an increase in the CuO content at the GB in the high-temperature sintering process.
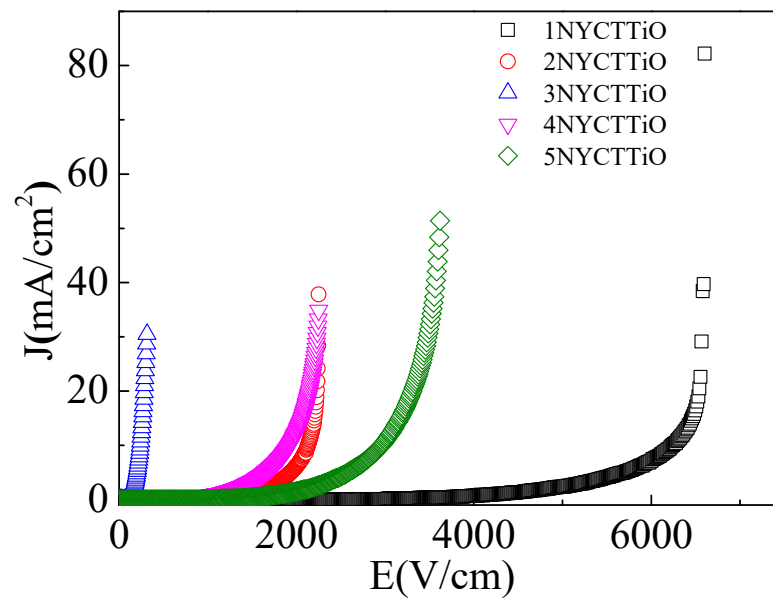
Figure 9. Nonlinear J-E characteristics of $Na_{1/2}Y_{1/2}Cu_3Ti_{4.1}O_{12}$ ceramics sintered at 1070 °C for 1, 5, and 15 h and sintered at 1080 and 1090 °C for 5 h.

The non-ohmic properties of NYCTO may be related to the oxygen concentration. Normally, R_{gb} can be increased by increasing the Ti and oxygen contents, which is a method for changing the non-ohmic properties of NYCTO ceramics [10,24]. However, the oxygen content was reduced by increasing the temperature. Therefore, the electrical resistance at the GBs of the $Na_{1/2}Y_{1/2}Cu_3Ti_{4.1}O_{12}$ ceramics might be decreased by this effect. However, the effect of changing the microstructure on non-ohmic properties should be considered.

4. Conclusions

The average grain sizes of the $Na_{1/2}Y_{1/2}Cu_3Ti_{4.1}O_{12}$ ceramics sintered under different conditions tended to increase slightly with sintering durations and temperatures. All major elements were detected in the microstructure, and the segregation of Cu and Ti was observed along the grain boundaries. The E_b and α values tended to decrease with increasing sintering durations. The $Na_{1/2}Y_{1/2}Cu_3Ti_{4.1}O_{12}$ ceramics sintered at 1070 °C for 1, 5, and 15 h and sintered at 1080 and 1090 °C for 5 h presented low and slightly changed tanδ values (0.009-0.025). The giant ε' increased with increasing sintering durations and sintering temperatures (5396–25,565). The impedance spectroscopy confirmed the IBLC structure in the $Na_{1/2}Y_{1/2}Cu_3Ti_{4.1}O_{12}$ ceramics, consisting of semi-Gs and i-GBs. The origin of n-type semiconducting grains was considered using the XPS results, and the existence of Cu^+, Cu^{3+}, and Ti^{3+} was detected. This result may have been caused by oxygen loss from the sintering duration and temperature process. The overall giant dielectric permittivity and electrical properties were described using Maxwell–Wagner relaxation polarization.

References

1. Wang, Y.; Jie, W.; Yang, C.; Wei, X.; Hao, J. Colossal Permittivity Materials as Superior Dielectrics for Diverse Applications. *Adv. Funct. Mater.* **2019**, *29*, 1808118. [CrossRef]
2. Pan, M.; Randall, C.A. A brief introduction to ceramic capacitors. *IEEE Electr. Insul. Mag.* **2010**, *26*, 44–50. [CrossRef]
3. Adams, T.; Sinclair, D.; West, A. Characterization of grain boundary impedances in fine- and coarse-grained $CaCu_3Ti_4O_{12}$ ceramics. *Phys. Rev. B* **2006**, *73*, 094124. [CrossRef]
4. Li, Y.; Li, W.; Du, G.; Chen, N. Low temperature preparation of $CaCu_3Ti_4O_{12}$ ceramics with high permittivity and low dielectric loss. *Ceram. Int.* **2017**, *43*, 9178–9183. [CrossRef]
5. Du, G.; Wei, F.; Li, W.; Chen, N. Co-doping effects of A-site Y^{3+} and B-site Al^{3+} on the microstructures and dielectric properties of $CaCu_3Ti_4O_{12}$ ceramics. *J. Eur. Ceram. Soc.* **2017**, *37*, 4653–4659. [CrossRef]
6. Yanchevskii, O.Z.; V'yunov, O.I.; Belous, A.G.; Kovalenko, L.L. Dielectric properties of $CaCu_3Ti_4O_{12}$ ceramics doped with aluminium and fluorine. *J. Alloys Compd.* **2021**, 159861. [CrossRef]
7. Mao, P.; Wang, J.; Xiao, P.; Zhang, L.; Kang, F.; Gong, H. Colossal dielectric response and relaxation behavior in novel system of Zr^{4+} and Nb^{5+} co-substituted $CaCu_3Ti_4O_{12}$ ceramics. *Ceram. Int.* **2021**, *47*, 111–120. [CrossRef]
8. Miao, G.; Yin, M.; Li, P.; Hao, J.; Li, W.; Du, J.; Li, G.; Wang, C.; Fu, P. Effect of Cr addition on the structure and electrical properties of $CaCu_3Ti_4O_{12}$ NTC thermistor. *J. Alloys Compd.* **2021**, *884*, 161066. [CrossRef]
9. Lin, Y.-H.; Cai, J.; Li, M.; Nan, C.-W.; He, J. High dielectric and nonlinear electrical behaviors in TiO_2-rich $CaCu_3Ti_4O_{12}$ ceramics. *Appl. Phys. Lett.* **2006**, *88*, 172902. [CrossRef]
10. Kotb, H.M.; Ahmad, M.M.; Alshoaibi, A.; Yamada, K. Dielectric Response and Structural Analysis of (A^{3+}, Nb^{5+}) Cosubstituted $CaCu_3Ti_4O_{12}$ Ceramics (A: Al and Bi). *Materials* **2020**, *13*, 5822. [CrossRef]
11. Schmidt, R.; Stennett, M.C.; Hyatt, N.C.; Pokorny, J.; Prado-Gonjal, J.; Li, M.; Sinclair, D.C. Effects of sintering temperature on the internal barrier layer capacitor (IBLC) structure in $CaCu_3Ti_4O_{12}$ (CCTO) ceramics. *J. Eur. Ceram. Soc.* **2012**, *32*, 3313–3323. [CrossRef]
12. Boonlakhorn, J.; Chanlek, N.; Manyam, J.; Srepusharawoot, P.; Krongsuk, S.; Thongbai, P. Enhanced giant dielectric properties and improved nonlinear electrical response in acceptor-donor (Al^{3+}, Ta^{5+})-substituted $CaCu_3Ti_4O_{12}$ ceramics. *J. Adv. Ceram.* **2021**, *10*, 1243–1255. [CrossRef]
13. Tuichai, W.; Danwittayakul, S.; Manyam, J.; Chanlek, N.; Takesada, M.; Thongbai, P. Giant dielectric properties of Ga^{3+}–Nb^{5+}Co-doped TiO_2 ceramics driven by the internal barrier layer capacitor effect. *Materialia* **2021**, *18*, 101175. [CrossRef]
14. Lin, Y.-H.; Cai, J.; Li, M.; Nan, C.-W.; He, J. Grain boundary behavior in varistor-capacitor TiO_2-rich $CaCu_3Ti_4O_{12}$ ceramics. *J. Appl. Phys.* **2008**, *103*, 074111. [CrossRef]
15. Thongbai, P.; Putasaeng, B.; Yamwong, T.; Maensiri, S. Current–voltage nonlinear and dielectric properties of $CaCu_3Ti_4O_{12}$ ceramics prepared by a simple thermal decomposition method. *J. Mater. Sci. Mater. Electron.* **2012**, *23*, 795–801. [CrossRef]
16. Liang, P.; Li, Y.; Zhao, Y.; Wei, L.; Yang, Z. Origin of giant permittivity and high-temperature dielectric anomaly behavior in $Na_{0.5}Y_{0.5}Cu_3Ti_4O_{12}$ ceramics. *J. Appl. Phys.* **2013**, *113*, 224102. [CrossRef]
17. Liang, P.; Li, Y.; Li, F.; Chao, X.; Yang, Z. Effect of the synthesis route on the phase formation behavior and electric property of $Na_{0.5}Bi_{0.5}Cu_3Ti_4O_{12}$ ceramics. *Mater. Res. Bull.* **2014**, *52*, 42–49. [CrossRef]
18. Peng, Z.; Wang, J.; Zhou, X.; Zhu, J.; Lei, X.; Liang, P.; Chao, X.; Yang, Z. Grain engineering inducing high energy storage in $CdCu_3Ti_4O_{12}$ ceramics. *Ceram. Int.* **2020**, *46*, 14425–14430. [CrossRef]
19. Peng, Z.; Liang, P.; Wang, J.; Zhou, X.; Zhu, J.; Chao, X.; Yang, Z. Interfacial effect inducing thermal stability and dielectric response in $CdCu_3Ti_4O_{12}$ ceramics. *Solid State Ionics* **2020**, *348*, 115290. [CrossRef]
20. Kotb, H.M.; Khater, H.A.; Saber, O.; Ahmad, M.M. Sintering Temperature, Frequency, and Temperature Dependent Dielectric Properties of $Na_{0.5}Sm_{0.5}Cu_3Ti_4O_{12}$ Ceramics. *Materials* **2021**, *14*, 4805. [CrossRef]
21. Saengvong, P.; Chanlek, N.; Putasaeng, B.; Pengpad, A.; Harnchana, V.; Krongsuk, S.; Srepusharawoot, P.; Thongbai, P. Significantly Improved Colossal Dielectric Properties and Maxwell—Wagner Relaxation of TiO_2—Rich $Na_{1/2}Y_{1/2}Cu_3Ti_{4+x}O_{12}$ Ceramics. *Molecules* **2021**, *26*, 6043. [CrossRef] [PubMed]
22. Liang, P.; Chao, X.; Yang, Z. Low dielectric loss, dielectric response, and conduction behavior in Na-doped $Y_{2/3}Cu_3Ti_4O_{12}$ ceramics. *J. Appl. Phys.* **2014**, *116*, 044101. [CrossRef]

23. Ahmad, M.; Mahfoz Kotb, H. Giant dielectric properties of fine-grained $Na_{1/2}Y_{1/2}Cu_3Ti_4O_{12}$ ceramics prepared by mechanosynthesis and spark plasma sintering. *J. Mater. Sci. Mater. Electron.* **2015**, *26*, 8939–8948. [CrossRef]

24. Liu, Z.; Jiao, G.; Chao, X.; Yang, Z. Preparation, microstructure, and improved dielectric and nonlinear electrical properties of $Na_{1/2}La_{1/2}Cu_3Ti_4O_{12}$ ceramics by sol–gel method. *Mater. Res. Bull.* **2013**, *48*, 4877–4883. [CrossRef]

25. Liu, Z.; Chao, X.; Yang, Z. Preparation process, microstructure and dielectric properties of $Na_{0.5}La_{0.5}Cu_3Ti_4O_{12}$ ceramics by a sol–gel method. *J. Mater. Sci. Mater. Electron.* **2014**, *25*, 2096–2103. [CrossRef]

26. Liang, P.; Chao, X.; Wang, F.; Liu, Z.; Yang, Z. The Lowered Dielectric Loss and Grain-Boundary Effects in La-doped $Y_{2/3}Cu_3Ti_4O_{12}$ Ceramics. *J. Am. Ceram. Soc.* **2013**, *96*, 3883–3890. [CrossRef]

27. Li, J.; Liang, P.; Yi, J.; Chao, X.; Yang, Z. Phase Formation and Enhanced Dielectric Response of $Y_{2/3}Cu_3Ti_4O_{12}$ Ceramics Derived from the Sol–Gel Process. *J. Am. Ceram. Soc.* **2015**, *98*, 795–803. [CrossRef]

28. Ahmad, M.M.; Kotb, H.M.; Joseph, C.; Kumar, S.; Alshoaibi, A. Transport and Dielectric Properties of Mechanosynthesized $La_{2/3}Cu_3Ti_4O_{12}$ Ceramics. *Crystals* **2021**, *11*, 313. [CrossRef]

29. Szwagierczak, D. Dielectric behavior of $Bi_{2/3}Cu_3Ti_4O_{12}$ ceramic and thick films. *J. Electr.* **2009**, *23*, 56–61. [CrossRef]

30. Jesus, L.M.; Silva, R.S.; Raj, R.; M'Peko, J.C. Electric field-assisted flash sintering of $Bi_{2/3}Cu_3Ti_4O_{12}$ starting from a multi-phase precursor powder. *J. Eur. Ceram. Soc.* **2020**, *40*, 4004–4009. [CrossRef]

31. Yang, Z.; Liang, P.; Yang, L.; Shi, P.; Chao, X.; Yang, Z. Synthesis, dielectric properties of $Bi_{2/3}Cu_3Ti_4O_{12}$ ceramics by the sol–gel method. *J. Mater. Sci. Mater. Electron.* **2015**, *26*, 1959–1968. [CrossRef]

32. Rajendar, V.; Rajitha, B.; Rao, K.V. Novel sol–gel method for synthesis of Bi2/3Cu3Ti4O12 (BCTO) and its light harvesting applications. *J. Mater. Sci. Mater. Electron.* **2015**, *26*, 9661–9666. [CrossRef]

33. Liang, P.; Li, Y.; Chao, X.; Yang, Z. Pseudo-relaxor behavior in $Na_{1/2}Bi_{1/2}Cu_3Ti_4O_{12}$ ceramics. *Mater. Res. Bull.* **2014**, *60*, 212–216. [CrossRef]

34. Ramezani, M.; Sobhani-Nasab, A.; Hosseinpour-Mashkani, S.M. Synthesis, characterization, and morphological control of $Na_{1/2}Bi_{1/2}Cu_3Ti_4O_{12}$ through modify sol–gel method. *J. Mater. Sci. Mater. Electron.* **2015**, *26*, 4848–4853. [CrossRef]

35. Li, W.; Tang, L.; Xue, F.; Xin, Z.; Luo, Z.; Du, G. Large reduction of dielectric losses of $CaCu_3Ti_4O_{12}$ ceramics via air quenching. *Ceram. Int.* **2017**, *43*, 6618–6621. [CrossRef]

36. Zeng, Y.; Rao, S.; Xiong, C.; Du, G.; Fan, Z.; Chen, N. Enhanced dielectric and mechanical properties of $CaCu_3Ti_4O_{12}/Ti_3C_2Tx$ MXene/silicone rubber ternary composites. *Ceram. Int.* **2022**, *48*, 6116–6123. [CrossRef]